Reaktor

p-ISSN 0852 – 0798
e-ISSN 2407 – 5973

Website: http://ejournal.undip.ac.id/index.php/reaktor/

Reaktor, Vol. 25 No. 3, December Year 2025, pp. 100-108

Production and Application of Carbon Dots from Sugarcane Bagasse-Derived-Lignin for Pb^{2+} Ion Detection

Berlian Sitorus[1*)], Dionisius Rio[1)], Intan Syahbanu[1)], Seno Darmawan Panjaitan[2)]

[1)]Department of Chemistry, Faculty of Mathematics and Natural Sciences, Universitas Tanjungpura, Jl. Prof. Dr. H. Hadari Nawawi, Pontianak, Indonesia
[1)]Department of Electrical Engineering, Faculty of Engineering, Universitas Tanjungpura, Jl. Prof. Dr. H. Hadari Nawawi, Pontianak, Indonesia

[*)]Corresponding author: berlian.sitorus@chemistry.untan.ac.id

(Received: 10 October 2025; Accepted: 11 December 2025; Published: 16 December 2025)

Abstract

This study investigates the manufacture and application of carbon dots derived from sugarcane bagasse lignin for lead ions detection. Lignin was extracted from bagasse through consecutive alkaline treatment and acid precipitation employing sodium hydroxide and sulfuric acid, respectively. Subsequently, the isolated lignin was converted into carbon dots through a hydrothermal process. Characterization revealed a particle size distribution of 7 ± 4 nm and distinctive absorbance peaks at 236, 317, and 360 nm in UV-Vis spectroscopy. To test their application in lead detection, the carbon dots are exposed to Pb^{2+} ions in concentrations of 0.01, 0.1, 1, and 10 µM. The carbon dots exhibited a notable fluorescence quenching response in the presence of Pb^{2+} ions. Photoluminescence spectroscopy confirmed that lead ions interact with the carbon dots, resulting in the reduction of their emission intensity. These findings demonstrate the potential of lignin-derived carbon dots as effective sensors for detecting Pb^{2+} ions.

Keywords: *carbon dots; hydrothermal; lead ion detection; lignin; sugarcane bagasse.*

How to Cite This Article: Sitorus, B., Rio, D., Syahbanu, I., Panjaitan, S.D. (2025), Production and Application of Carbon Dots from Sugarcane Bagasse-Derived-Lignin for Pb^{2+} Ion Detection, Reaktor, 25 (3), 100–108, https://doi.org/10.14710/reaktor.25.3.100-108

INTRODUCTION

Sugarcane bagasse, a biomass waste rich in lignin (22.4%), cellulose (45.3%), and hemicellulose (22.1%) contents, offers a promising source for carbon dot (CD) synthesis (Yao *et al.,* 2015). Lignin, often discarded as a byproduct in the pulp and paper industry, presents an underutilized resource with significant economic and environmental implications (Yuan *et al.,* 2021). The abundance of hydroxyl phenol groups and ethers within lignin makes it a potential precursor for CD production. The unique properties of lignin-derived CDs, including their ability to electrostatically interact with heavy metals, suggest

their potential application in sensor technology (Sun *et al.,* 2019).

Various factors that influence the formation of carbon dots, including temperature and reaction duration. The carbonization process, which requires temperature exceeding 100°C, involves dehydration and carbonization. The reaction duration can be monitored by observing the color change of the precursor solution. Optimal carbon dot production typically results in yellow, orange, or brown solutions. Insufficient reaction time may prevent discoloration, while excessive treatment can lead to solution darkening and loss of carbon dot fluorescence. In addition to these factors, the choice of carbon source has a significant impact on carbon dot production. Lignin offers advantages such as high carbon content and a favorable structural composition.

Previous studies have explored the synthesis of carbon dots from various types of lignin, including their application in metal-ion sensing, specifically for Fe^{3+} detection (Guo *et al*., 2022). However, research involving sugarcane bagasse lignin as a precursor for carbon dot synthesis remains limited, and no study has applied such materials for Pb^{2+} ion detection. This work contributes to fill that gap by introducing carbon dots synthesized from bagasse-derived lignin and evaluating their performance as fluorescent probes for Pb^{2+} sensing. The successful development of carbon dots from bagasse lignin could contribute to advancements in materials science and enhance the economic value of bagasse waste.

MATERIALS AND METHODS

Materials

Materials employed in this study included distilled water (H_2O), bagasse, 95-97% sulfuric acid (H_2SO_4), filter paper, standard lignin (Sigma-Aldrich), sodium hydroxide (NaOH) (Merck 106498), and lead (II) nitrate ($PbNO_3$) (Emsure).

Laboratory Apparatus

General laboratory glassware, such as beakers, flasks, pipettes, a blender, a 100-mesh sieve, a hot plate stirrer, a centrifuge, an analytical balance, a reflux apparatus, a spatula, a bulb pipette, universal indicator paper, a static discharger, and a 0.20-µm CHROMAFIL Xtra PA (Nylon) 25-mm syringe filter were used during the experiments. Meanwhile, a Teflon-lined stainless-steel autoclave was utilized for hydrothermal synthesis.

Methods

Pretreatment of Sugarcane Bagasse

Prior to use as a raw material, sugarcane bagasse was thoroughly washed with flowing water and subsequently air-dried for 4-5 days before cut into small pieces. Following this, the bagasse was subjected to size reduction step using a blender and further sieved through a 100-mesh sieve. Before lignin isolation, 20 grams of 100-mesh bagasse powder was boiled for 2 hours at 70°C in deionized water at a 1:10 ratio. The boiled bagasse was then filtered to separate any water-soluble impurities (Arni, 2018).

Isolation of Lignin from Sugarcane Bagasse

Lignin isolation from bagasse was carried out through a chemical process utilizing a 16% NaOH solution according to the alkaline treatment method. The pretreated bagasse was refluxed with 200 mL of 16% sodium hydroxide (4 M concentration) at 98°C for 90 minutes, maintaining a 1:10 ratio of bagasse powder to sodium hydroxide. The resulting black liquor mixture was cooled to 25°C and then filtered to separate the hemicellulose-containing filtrate from the solid residue. The filtrate was subsequently added with 1.5 M H_2SO_4 to a pH of 2 to facilitate precipitation. The precipitate was separated from the mixture using centrifugation, washed, and dried in an oven at 60°C to completely diminish the residual moisture, yielding lignin powder. The lignin yield was calculated using Equation 1 (Mennani *et al*., 2022).

$$\text{Lignin yield (\%)} = \frac{w_1}{w_2} \text{x} 100\% \ldots\ldots\ldots\ldots (1)$$

W_0 = mass of sugarcane bagasse powder (g)
W_1 = mass of lignin produced from sugarcane bagasse (g)

Formation and Characterization of Carbon Dots

Two grams of lignin were mixed with 30 mL of distilled water in a 100 mL Teflon-lined stainless-steel autoclave. The lignin-water mixture underwent a hydrothermal process at 180°C for 8 hours, resulting in a color change. The autoclave was then equilibrated to room temperature, and the colored solution was filtered using filter paper with the help of a 0.20 µm filter syringe. The filtrate was subsequently stored in a dark bottle at a low temperature for future use (Kumar *et al*., 2017).

The carbon dots obtained were characterized using a particle size analyzer (PSA), irradiated under a 365 nm UV lamp, and subjected to UV-Vis spectroscopy. The particle size distribution was determined using the Horiba-100 nanoparticle analyzer. The carbon dots exhibited fluorescence under irradiation from a 365 nm UV lamp. The maximum emission wavelength of the carbon dots was measured using UV-Vis spectroscopy within a wavelength range of 200-600 nm.

Characterization Techniques

a) Lignin Characterization

The isolated lignin was characterized using Fourier-transform infrared spectroscopy (FTIR). The characterization was carried out using a Shimadzu FTIR 8400 spectrophotometer over the wavenumber range of 4000–500 cm^{-1} with a resolution of 4 cm^{-1}. To minimize possible interference from moisture, KBr pellets were prepared and dried in an oven prior to analysis.

(b) Carbon Dot Characterization

The synthesized carbon dots were subjected to multiple characterization techniques. Particle size distribution was determined using a Horiba SZ-100 nanoparticle analyzer (PSA). Fluorescence behavior was evaluated by irradiating the samples under a 365 nm UV lamp to observe photoluminescence response. UV–Vis absorbance spectra were recorded using a Shimadzu UV-2600 UV–Vis spectrophotometer within the wavelength range of 200–600 nm. Photoluminescence (PL) spectra were obtained using an Agilent Cary Eclipse fluorescence spectrometer.

Pb^{2+} Detection Test Procedure

Carefully prepared Pb^{2+} solutions with concentrations of 0.01, 0.1, 1.0, and 10 µM were prepared from a 10 µM stock solution. Each Pb^{2+} solution (0.75 mL) was added to 3 mL of the carbon dot solution, mixed thoroughly, and allowed to stand for 15 minutes. The mixtures were then photographed under a 365 nm UV lamp to observe fluorescence changes. The presence of Pb^{2+} resulted in fluorescence quenching, which was confirmed by the decrease in photoluminescence (PL) intensity at an excitation wavelength of 450 nm (Kumar *et al*., 2017).

RESULTS AND DISCUSSION

Pretreated Bagasse Characteristics

The pretreatment process produced a fine, homogeneous bagasse powder with a bright, light-colored appearance, as shown in Figure 1. The uniformity of the 100-mesh particles indicates effective mechanical size reduction and a substantial increase in accessible surface area, which is beneficial for enhancing the efficiency of lignin isolation. The lighter color of the powder also suggests the successful removal of water-soluble impurities, extractives, and part of the hemicellulose fraction during the hot-water washing stage. This purification effect is consistent with previous findings, which report that thermal water extraction at moderate temperatures effectively removes non-structural components and improves lignocellulosic purity (Boussetta *et al*., 2021; Mennani *et al*., 2022). The resulting pretreated bagasse therefore provides a cleaner and more reactive substrate, supporting more efficient lignin isolation in the subsequent extraction step.

Figure 1. The 100-mesh bagasse after treatment.

Isolation of Lignin from Sugarcane Bagasse

The alkaline treatment resulted in an apparent increase in lignin solubility, demonstrating its effectiveness in disrupting the lignocellulosic matrix of sugarcane bagasse. This behavior is consistent with previous reports, which claim that alkaline conditions promote the cleavage of lignin – carbohydrate linkages and facilitate the liberation of lignin into solution (Boussetta *et al*., 2021; Mennani *et al*., 2022). Following the treatment, the isolated lignin exhibited a black-brown appearance, as shown in Figure 2, which is characteristic of alkali-extracted lignin from agricultural residues. Sodium hydroxide is widely recognized as an efficient alkali for lignin extraction, often yielding higher lignin recovery than KOH within the commonly reported optimal concentration range of 10–15%. At this level, NaOH selectively solvates lignin while retaining the structure of cellulose and hemicellulose, reflecting the well-established selectivity of alkaline delignification. Overall, the response of bagasse to alkaline treatment in this study aligns well with literature trends, confirming that NaOH provides suitable conditions for obtaining lignin of adequate purity for subsequent carbon dot synthesis.

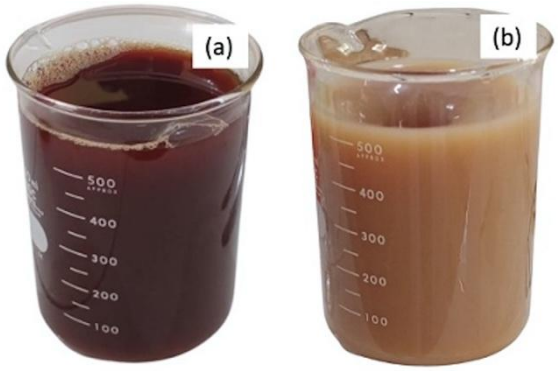

Figure 2. Black and brown lignin obtained from black liquor: (a) black liquor solution after pulping process and (b) brown liquor solution, adjusted to pH 2, showing brown liquor and lignin precipitation.

Under alkaline conditions, hydroxyl ions deprotonate the phenolic hydroxyl groups of lignin, generating phenolate ions that increase the susceptibility of ether linkages, particularly β-O-4 bonds, to cleavage. The breaking of these linkages produces smaller phenolic fragments with higher water solubility, supported by the negative charge introduced through phenolate formation (Yuan *et al*., 2021; Deuss *et al*., 2018). As these fragments dissolve into the NaOH solution, lignin is effectively separated from the cellulose and hemicellulose components of the biomass.

Following acidification, the lignin coagulated and formed a dense, cohesive mass that settled readily from the black liquor.

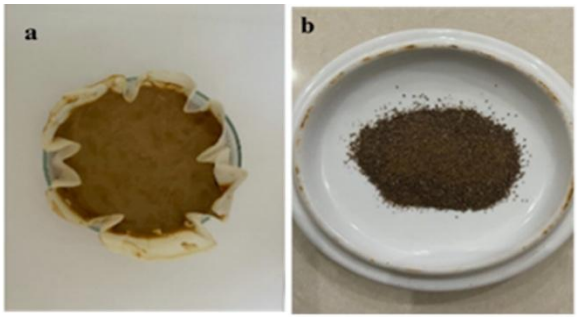

Figure 3. Lignin obtained after precipitation and drying: (a) wet lignin filtered after acid settling and (b) dry lignin after oven drying.

After filtration, the material appeared as a thick, dark-brown precipitate (Figure 3a), indicating successful coagulation and separation from the aqueous phase. Upon drying, the lignin transformed into a fine, granular powder with a more uniform texture and reduced moisture content (Figure 3b). This transition from a wet, compact precipitate to a dry particulate solid is characteristic of sulfuric-acid precipitated lignin and reflects the removal of residual water and soluble impurities during the drying stage. The final lignin yield obtained in this study was 15.3 ± 2.5% across three replicates, which falls within the expected range for alkali-extracted lignin from sugarcane bagasse.

Isolation of Lignin from Sugarcane Bagasse

The Fourier transform infrared (FTIR) spectra of bagasse, isolated lignin, and commercial lignin, as shown in Figure 4, revealed unique characteristic peaks consistent with the literature, confirming the distinctive structural features of lignin. The bagasse spectrum exhibited prominent peaks indicative of lignocellulosic components, including cellulose, hemicellulose, and lignin. A distinct peak confirmed the presence of lignin at 1120 – 1220 cm^{-1}, attributed to the C-O stretching vibration of the ester group within the p-hydroxy phenyl propane (H), guaiacyl (G), and syringyl (S) units (Kalami *et al.*, 2017). Additional characteristic peaks at 1593-1604 cm^{-1}, 1510 – 1514 cm^{-1}, 1265 cm^{-1}, 1458 – 1463 cm^{-1}, and 1417-1429 cm^{-1} supported the presence of lignin and its aromatic structure (Chen *et al.*, 2019; Kalami *et al.*., 2017; Ma *et al.*, 2020). Moreover, the broad band at 3414 – 3450 cm^{-1} and peaks at 2839 – 2935 cm^{-1} indicated the presence of hydroxyl groups and aliphatic C-H bonds. The observed peaks at 1635 – 1643 cm^{-1} suggested the formation of hydrogen bonds between carbonyl groups and water molecules, as previously reported (Kalami *et al.*, 2017).

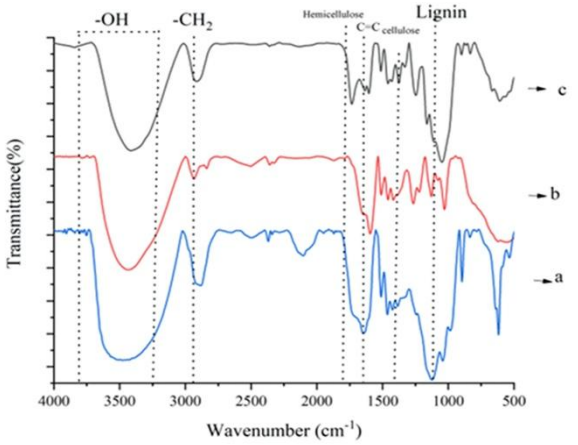

Figure 4. Comparison of FTIR spectra: (a) isolated lignin, (b) commercial lignin, and (c) bagasse.

The FTIR spectrum of lignin exhibited a new peak at 617 cm^{-1}, indicative of S-O and C-S bond stretching vibrations. This peak is likely due to the previous sulfuric acid (H_2SO_4) treatment during lignin isolation from black liquor (Menn *et al* ani, 2022). In addition to this new peak, the lignin spectrum exhibited a characteristic peak at 1028 – 1080 cm^{-1}, corresponding to C-H deformation vibrations within the guaiacyl unit (Ma *et al*., 2020). A peak at 1384 – 1388 cm^{-1} is attributed to the aliphatic C-H deformation vibration of the phenolic (OH) group, a feature specific to lignin and commercial lignin (Boussetta *et al.*, 2021). A peak at 835 cm^{-1} in both the bagasse and lignin spectra suggests the existence of C-H bond vibrations in the substituted aromatic ring (Bhagia *et al.*, 2022). Peaks at 1244 – 1246 cm^{-1} indicate the presence of lignin derived from the aromatic ester of syringyl lignin (Bolio *et al*, 2016). Notably, the absence of peaks at 665, 1246, 1375, and 1734 cm^{-1} in the lignin spectrum confirms the complete removal of hemicellulose and cellulose components during the lignin isolation process.

Carbon Dots Formation

The use of water as a solvent in carbon dot production aligns with the pursuit of environmentally friendly approaches. Hydrothermal carbonization typically occurs within a temperature range of 120 – 200°C, with optimal absorption and emission observed at 180°C. The process temperature significantly influences the carbon dot structure, with appropriate temperatures leading to a more uniform size distribution. Too high carbonization temperatures can result in larger carbon dots due to irregular growth. A homogeneous size distribution contributes to a narrower distribution of energy levels, which in turn affects the light absorption and emission spectrum. This ultimately results in sharper and clearer fluorescence, facilitating observation under UV light and measurements using UV-Vis spectroscopy (Kumar *et al.*, 2017).

During the hydrothermal process, the color of the solution changed to yellow, indicating the completion of carbonization. The duration of carbonization can influence the final color of the carbon dots, with both yellow and brown being common. In addition to carbonization time, the choice of carbon precursors plays a crucial role in determining fluorescence intensity and photoluminescent color regulation. The presence of oxygen-containing groups, such as -OCH_3 and -OH, in lignin precursors creates active sites on the surface of carbon dots, enabling them to regulate photoluminescence properties and enhance light emission (Guo *et al.*, 2022).

The formation of carbon dots commences with the ionization of water to form H^+ ions at temperatures exceeding 100°C. Under the influence of these protons, the β-aryl-ether (β-O-4) linkages within the lignin structure undergo cleavage, generating carbocations concurrently. This carbocation formation initiates the depolymerization of lignin into smaller aromatic molecules (monomers). The visual evidence of this process is the observed color change from an initially heterogeneous and turbid mixture of lignin and water (Figure 5a) to a homogeneous yellow solution (Figure 5b).

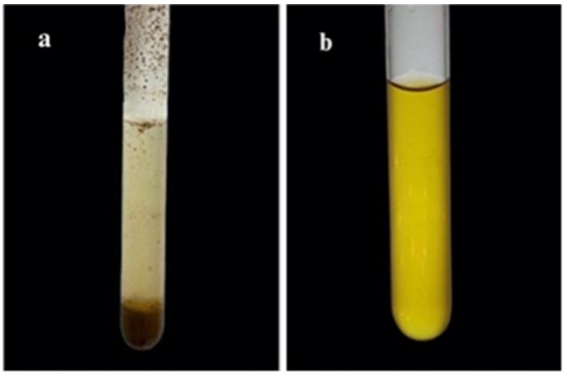

Figure 5. A visual comparison of the lignin solution: (a) before and (b) after the formation of carbon dots

As previously described by Han *et al.* (2022), as the depolymerization of lignin progresses, carbocations continue to form as intermediate products. These electrophilic carbocations can then react with the electron-rich carbon atoms within the aromatic phenyl rings of lignin fragments (via aldol condensation and cycloaddition), forming aromatic fragments. When the concentration of these aromatic fragments reaches a critical saturation point, nucleation and phase separation occur, forming lignin-derived carbon dots as in Figure 5b.

Carbon dots are formed from lignin through a sequence of thermally driven depolymerization, aromatization, and carbonization steps. During heating, the predominant β-O-4 ether linkages in lignin cleave to produce smaller phenolic fragments, which subsequently undergo dehydration, deoxygenation, and condensation to form polyaromatic clusters. These clusters then serve as nuclei for the growth of carbonaceous nanoparticles, which are further functionalized by residual oxygen-containing groups from the lignin precursor (Chen *et al.*, 2021). These clusters nucleate and grow into sp^2-rich carbon cores, while the original oxygen-containing groups of lignin (–OH, –COOH, –O–) are partially retained on the particle surface, acting as natural passivating agents.

Carbon Dots Characterization

Characterization of the carbon dots solution using the UV-Vis Spectrophotometer instrument was successfully carried out. In the characterization using the UV-Vis instrument, the analysis results showed a typical absorbance peak in a certain wavelength range. The analysis result can be seen in Figure 6. This absorbance peak is characteristic of carbon dots, indicating the successful synthesis of the material.

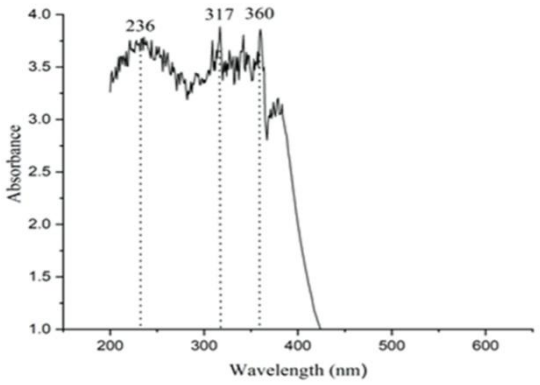

Figure 6. The UV-Vis spectrum of Carbon dots

The peak at 236 nm is associated with the π-π* electronic transition of conjugated unsaturated structures (-C=C-C=O) or C=C bonds on aromatic rings. The CD shows a red shift. The reason is that lignin is acidic, as carbon dots are obtained at a pH of 3. Lignin, as a precursor of CD contains many phenolic groups. Under acidic conditions, phenolic groups can undergo protonation, altering the electronic structure of the CD surface and causing longer wavelength shifts. This property of lignin acid is caused by the interaction of lignin with sulfuric acid before the sedimentation process is carried out after lignin isolation. The acidic nature changes the energy level of the CD electronics, which can affect light absorption. A peak of 317 nm is also caused by the n-π* electronic transition of the C=O bond in the CD.

The peak of 317 nm experienced a redshift. Acids affect the amount of phenolic (ester groups) in lignin. The more acidic it is, the more phenolic in lignin will be reduced, so that it will cause a longer wavelength shift. There is also an absorption peak at 360 nm, which comes from the transition of n-π* between groups containing sp^2 domains, such as double bonds in aromatic compounds and carbonyl bonds (C=O) in the structure of CD (L. Sun et al., 2021).

Further, particle size analysis was conducted to determine the particle size distribution of the synthesized carbon dots. The results, as Z-average, are presented in Table 1. The particle size of carbon dots is directly correlated with their average molecular weight. Lignin precursors with higher molecular weights tend to form larger particles. Additionally, the hydrophilic nature of lignin is influenced by its molecular weight.

As indicated in Table 1 and Figure 7, the synthesized carbon dots exhibited a mean z-average particle size of 7.43 nm. The presence of hydroxyl (-OH) functional groups in lignin significantly impacts its molecular weight and, consequently, the size of the resulting carbon dots. Lignin with a lower concentration of hydroxyl groups exhibits a smaller molecular weight and tends to be more hydrophobic, forming smaller nanoparticles (Ma *et al.*., 2020).

Table 1. The characteristic size of synthesized carbon dots

Repetition	Z-Average (nm)	Mode (nm)	Polydispersity Index (PI) (%)
1	2.8	25.8	0.687
2	10	11.0	0.773
3	9.5	6.0	1.202
Mean	7.43	14.27	0.887

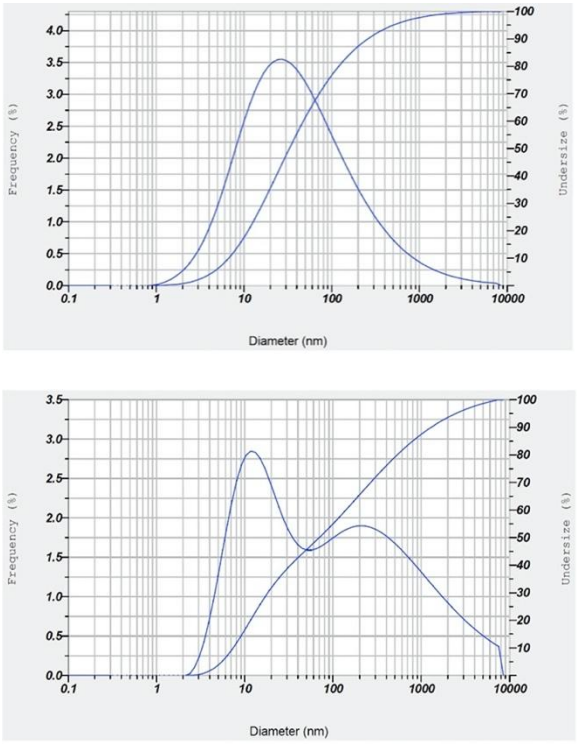

Figure 7. Particle size distribution of the synthesized carbon dots according to DLS

Carbon Dots for Detection of Pb^{2+}

The detection efficiency of the carbon dots was evaluated by exposing them to aqueous solutions containing varying concentrations of lead ions (0.01-10 µM). Fluorescence testing was conducted under irradiation from a 365 nm UV lamp. As depicted in Figure 9, the carbon dots exhibited blue fluorescence in the absence of lead ions or at very low Pb^{2+} concentrations. However, upon the addition of Pb^{2+} ions 0.1 µM (Figures 8(c), (d), and (e)), the blue fluorescence was quenched.

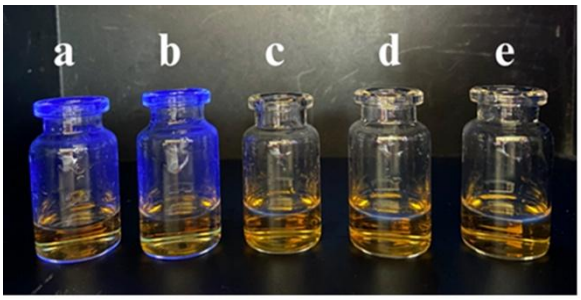

Figure 8. Fluorescence imaging of carbon dots under 365 nm UV Irradiation :(a) control (carbon dots only), (b) 0.01 µM Pb^{2+}, (c) 0.1 µM Pb^{2+}, (d)1 µM Pb^{2+}, and (e) 10 µM Pb^{2+}.

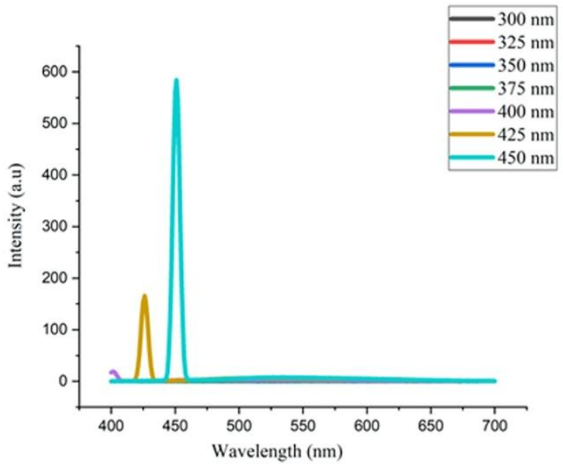

Figure 9. Excitation spectra of the synthesized carbon dots.

The fluorescence intensity of the obtained carbon dots varied with excitation wavelength, reaching a maximum at 450 nm when the excitation wavelength was scanned from 300 nm to 450 nm, as shown in Figure 9. When emission was measured at 450 nm, the maximum emission intensity was found at 550 nm (Figure 10). The observed fluorescence quenching is attributed to the interaction between lead ions and the phenolic groups on the surface of the carbon dots. The electron-withdrawing nature of lead ions leads to the formation of a non-fluorescent complex by attracting electrons from the phenolic groups, thus altering the electron distribution.

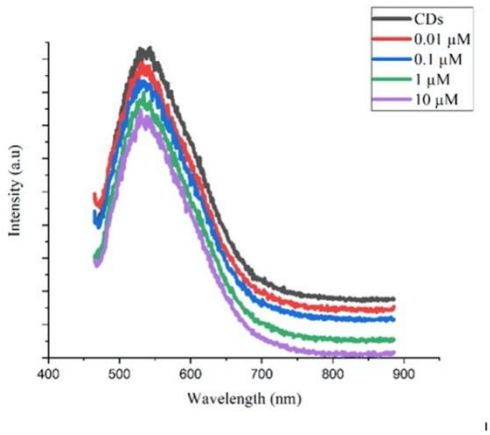

Figure 10. Effect of Pb^{2+} ion concentration on the emission intensity of carbon dots.

The degree of fluorescence quenching was directly correlated with the concentration of lead ions, demonstrating the sensitivity of the carbon dots for lead ion detection. Higher lead ion concentrations resulted in a more pronounced decrease in fluorescence intensity due to the increased number of phenolic groups interacting with lead ions (Plácido *et al.*, 2019). In conclusion, the carbon dots exhibited a clear response to lead ions within the concentration range of 0.1-10 µM, as evidenced by the loss of blue fluorescence. The observed fluorescence quenching mechanism is consistent with the interaction between lead ions and the phenolic groups on the carbon dot surface.

Mechanism of Pb^{2+} ions sensing by CDs

Although numerous mechanisms have been proposed to explain metal-ion sensing by carbon dots (CDs), the exact quenching pathway remains an active topic of debate within the relevant scientific community (Kanwal *et al.*, 2022). Previous studies reported several possible quenching routes, including electron transfer, the inner filter effect (IFE), and the formation of non-fluorescent complexes between CDs and metal ions (Sugiarto *et al.*, 2023). The dominant mechanism generally depends on the interaction between the specific metal ion and the surface chemistry of the CDs, with different CD–metal combinations exhibiting distinct quenching behaviors (Plácido *et al.*, 2019). For instance, the quenching of CD photoluminescence by Pb^{2+} has frequently been attributed to the strong affinity between the empty orbitals of Pb^{2+} and electron-rich ligands on the CD surface, which promotes non-radiative electron–hole recombination (Dhariwal *et al.*, 2023).

In the present work, however, both the FTIR signatures of the lignin precursor and the fluorescence quenching trends strongly indicate that coordination-driven static quenching is the predominant sensing mechanism (Sekar *et al.*, 2020). The FTIR spectrum confirms the presence of oxygen-containing functional groups—particularly phenolic –OH, carboxyl –COOH, and ether –O– groups—which are known to partially persist after carbonization and remain accessible on the surface of lignin-derived CDs. These electron-rich groups provide ideal binding sites for Pb^{2+}, a soft Lewis acid with high affinity for oxygen donor atoms. Upon interaction, Pb^{2+} forms coordination bonds with these surface functionalities, yielding a ground-state, non-fluorescent CD–Pb^{2+} complex.

This complexation not only alters the emissive surface states, but may also promote partial aggregation of the CDs, further enhancing fluorescence quenching (Shen *et al.*, 2021; Kanwal *et al.*, 2022). The observed concentration-dependent decrease in photoluminescence intensity, characterized by rapid quenching even at low Pb^{2+} concentrations, corroborates the suitability of these CDs for metal-ion sensing (Ang *et al.*, 2020). Static quenching typically arises from the formation of stable, non-emissive complexes in the ground state (Kanwal *et al.*, 2022), which reduces the population of photoexcited species available for radiative recombination (Panáček *et al.*, 2022).

The mechanistic interpretation is further supported by experimental observations: (i) a substantial, concentration-dependent decline in fluorescence intensity upon Pb^{2+} addition, (ii) pronounced quenching at Pb^{2+} concentrations as low as 0.1 µM, and (iii) the absence of spectral distortion or peak shifts, which excludes IFE and LIET as major contributors. The strong affinity between Pb^{2+} and the oxygenated surface ligands of the CDs significantly enhances the sensing sensitivity, enabling low detection limits (Wang *et al.*., 2021). Static quenching is also consistent with the fact that fluorescence suppression occurs due to complex formation before photoexcitation, leading to the inhibition of radiative decay pathways, a hallmark feature of static quenching mechanisms (Ren *et al.*, 2023).

Most carbon-dot–based metal ion sensors rely on fluorescence quenching, in which metal ions interact with surface functional groups of the carbon dots and reduce their emission (Zhang *et al.*, 2022). In this work, the quenching behavior is interpreted to obey a static quenching pathway, and the mechanism proposed in this study involves the formation of a ground-state, non-fluorescent complex between Pb^{2+} and the C-dots prior to excitation. The proposed mechanism is illustrated in Figure 11.

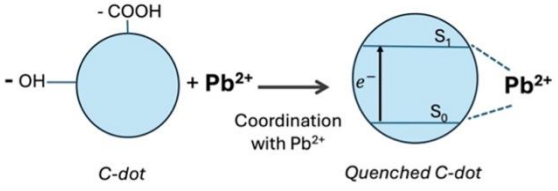

Figure 11. Proposed mechanism of lignin-derived carbon dots (C-dots) upon interaction with Pb^{2+} ions.

CONCLUSION

Based on the findings of this research, a successful isolation of lignin from bagasse has been achieved using an alkaline treatment with 16% NaOH, yielding a product with a purity of 15.3 ± 2.5%. FTIR analysis confirmed the presence of characteristic lignin functional groups, aligning with commercial lignin standards. The isolated lignin was successfully converted into carbon dots, yielding a yellow, fluorescent solution with an average diameter of 7.43 nm. A mechanism for detecting lead ions using these carbon dots was proposed, involving the interaction between lead ions and the functional groups on the surface of the carbon dots. Adding lead ions led to a quenching of the blue fluorescence emitted under 365 nm UV irradiation, with a proportional decrease in emission intensity as the lead ion concentration increased.

CONFLICT OF INTEREST

The authors declare that they have no conflict of interest.

ACKNOWLEDGEMENTS

The authors (BS and IS) gratefully acknowledge the financial support provided by Fakultas MIPA Universitas Tanjungpura through DIPA FMIPA research grant number 2799/UN22.8/PT.001.05/2024.

REFERENCES

Ang, W. L., Mee, C. A. L. B., Sambudi, N. S., Mohammad, A. W., Leo, C. P., Mahmoudi, E., Ba-Abbad, M. M., & Benamor, A. (2020). Microwave-assisted conversion of palm kernel shell biomass waste to photoluminescent carbon dots. Scientific Reports, 10 (1). https://doi.org/10.1038/s41598-020-78322-1

Arni, S.A., (2018), Extraction and isolation methods for lignin separation from sugarcane bagasse: A review, Industrial Crops and Products, 115, pp. 330–339. https://doi.org/10.1016/j.indcrop.2018.02.012

Bhagia, S., Ďurkovič, J., Lagaňa, R., Kardošová, M., Kačík, F., Cernescu, A., Schäfer, P., Yoo, C.G. and Ragauskas, A.J., (2022), Nanoscale FTIR and mechanical mapping of plant cell walls for understanding biomass deconstruction, ACS Sustainable Chemistry and Engineering, 10(9), pp.3016–3026. https://doi.org/10.1021/acssuschemeng.1c08163

Bolio, G.I., Veleva, L., Mateo, M. and Villegas, H., (2016), Extraction and characterization of cellulose from agroindustrial waste of pineapple (Ananas comosus L. Merrill) crowns, Chemical Science Review and Letters, 5, pp. 198–204.

Boussetta, A., Benhamou, A.A., Barba, F.J., Idrissi, M.E., Grimi, N. and Moubarik, A., (2021), Experimental and theoretical investigations of lignin-urea-formaldehyde wood adhesive: Density functional theory analysis, International Journal of Adhesion and Adhesives, 104, 102737. https://doi.org/10.1016/j.ijadhadh.2020.102737

Chen, Y., Gong, X., Yang, G., Li, Q. and Zhou, N., (2019), Preparation and characterization of a nanolignin phenol formaldehyde resin by replacing phenol partially with lignin nanoparticles, RSC Advances, 9(50), pp. 29255–29262. https://doi.org/10.1039/c9ra04827h

Chen, X., Zhu, J., Song, W., & Xiao, L. (2021), Integrated Cascade Biorefinery Processes to Transform Woody Biomass Into Phenolic Monomers and Carbon Quantum Dots. *Frontiers in Bioengineering and Biotechnology, 9*, 803138. https://doi.org/10.3389/fbioe.2021.803138

Dhariwal, J., Rao, G. K., & Vaya, D. (2023). Recent advancements towards the green synthesis of carbon quantum dots as an innovative and eco-friendly solution for metal ion sensing and monitoring. RSC Sustainability, 2(1), 11. https://doi.org/10.1039/d3su00375b

Guo, J., Xu, J., Liu, X., Dai, L., Zhang, C., Xiao, X., and Huo, K. (2022), Enabling dual valorization of lignocellulose by fluorescent lignin carbon dots and biochar-supported persulfate activation: Towards waste-treats-pollutant, Journal of Hazardous Materials, 435, 129072. https://doi.org/10.1016/j.jhazmat.2022.129072

Han, Y., Huang, X., Liu, J., Ni, J., Bai, Y., Zhao, B., Han, S. and Zhang, C., (2022), Seeking eye protection from biomass: Carbon dot-based optical blocking films with adjustable levels of blue light blocking, Journal of Colloid and Interface Science, 617, pp. 44–52. https://doi.org/10.1016/j.jcis.2022.02.115

Kalami, S., Arefmanesh, M., Master, E. and Nejad, M., (2017), Replacing 100% of phenol in phenolic adhesive formulations with lignin, Journal of Applied Polymer Science, 134(30), 45124. https://doi.org/10.1002/app.45124

Kanwal, A., Bibi, N., Hyder, S., Muhammad, A., Ren, H., Liu, J., & Lei, Z. (2022). Recent advances in green carbon dots (2015–2022): synthesis, metal ion sensing, and biological applications, Beilstein Journal of Nanotechnology, 13, 1068. Beilstein Institute for the Advancement of Chemical Sciences. https://doi.org/10.3762/bjnano.13.93

Kumar, A., Chowdhuri, A.R., Laha, D., Mahto, T.K., Karmakar, P. and Sahu, S.K., (2017), Green synthesis of carbon dots from Ocimum sanctum for effective fluorescent sensing of Pb^{2+} ions and live cell imaging, Sensors and Actuators B: Chemical, 242, pp. 679–686. https://doi.org/10.1016/j.snb.2016.11.109

Ma, M., Dai, L., Xu, J., Liu, Z. and Ni, Y., (2020), A simple and effective approach to fabricate lignin nanoparticles with tunable sizes based on lignin fractionation, Green Chemistry, 22(6), pp. 2011–2017. https://doi.org/10.1039/d0gc00377h

Mennani, M., Ait Benhamou, A., Kasbaji, M., Boussetta, A., Ablouh, E.H., Kassab, Z., El Achaby, M., Boussetta, N., Grimi, N. and Moubarik, A., (2022), Insights on the physico-chemical properties of alkali lignins from different agro-industrial residues and their use in phenol-formaldehyde wood adhesive formulation, International Journal of Biological Macromolecules, 221, pp. 149–162. https://doi.org/10.1016/j.ijbiomac.2022.08.191

Panáček, D., Zdražil, L., Langer, M., Šedajová, V., Baďura, Z., Zoppellaro, G., Yang, Q., Nguyen, E. P., Álvarez-Diduk, R., Hrubý, V., Kolařík, J., Chalmpes, N., Bourlinos, A. B., Zbořil, R., Merkoçi, A., Bakandritsos, A., & Otyepka, M. (2022), Graphene Nanobeacons with High-Affinity Pockets for Combined, Selective, and Effective Decontamination and Reagentless Detection of Heavy Metals. *Small*, *18*(33). https://doi.org/10.1002/smll.202201003

Plácido, J., Bustamante-López, S., Meissner, K.E., Kelly, D.E. and Kelly, S.L., (2019), Microalgae biochar-derived carbon dots and their application in heavy metal sensing in aqueous systems, Science of the Total Environment, 656, pp. 531–539. https://doi.org/10.1016/j.scitotenv.2018.11.393

Ren, H., Labidi, A., Sun, J., Allam, A. A., Ajarem, J. S., Abukhadra, M. R., & Wang, C. (2023), Green and facile synthesis of N,S co-doped carbon quantum dots with a high product yield for selective detection of Hg2+ in aqueous system. *Research Square (Research Square)*. https://doi.org/10.21203/rs.3.rs-2930575/v1

Sekar, A., Yadav, R., & Nivetha, B. (2020). Fluorescence quenching mechanism and the application of green carbon nanodots in the detection of heavy metal ions: a review [Review of Fluorescence quenching mechanism and the application of green carbon nanodots in the detection of heavy metal ions: a review]. New Journal of Chemistry, 45(5), 2326. Royal Society of Chemistry. https://doi.org/10.1039/d0nj04878j

Shen, Y., Wu, H., Li, J., Liu, G., Xiao, Y., Dai, Z., & Zhen, H. (2021). One-step hydrothermal method for preparing carbon dots and its determination of lead (II). Journal of Physics Conference Series, 2011(1), 12101. https://doi.org/10.1088/1742-6596/2011/1/012101

Sugiarto, I. T., Yulianto, N., Tresna, W. P., Lewa, I. W. L., & Isnaeni, I. (2023). Optical Response of Various Heavy Metal Ions-Based Carbon Dots Photoluminescent Quenching Effect, Journal of Physics and Its Applications, 6(1), 11. https://doi.org/10.14710/jpa.v6i1.18755

Sun, L., Mo, Z., Li, Q., Zheng, D., Qiu, X. and Pan, X., (2021), Facile synthesis and performance of pH/temperature dual-response hydrogel containing lignin-based carbon dots, International Journal of Biological Macromolecules, 175, pp. 516–525. https://doi.org/10.1016/j.ijbiomac.2021.02.049

Sun, X.F., Hao, Y., Cao, Y. and Zeng, Q., (2019), Superadsorbent hydrogel based on lignin and montmorillonite for Cu(II) ions removal from aqueous solution, International Journal of Biological Macromolecules, 127, pp. 511–519. https://doi.org/10.1016/j.ijbiomac.2019.01.058

Yao, S., Nie, S., Yuan, Y., Wang, S. and Qin, C., (2015), Efficient extraction of bagasse hemicelluloses and characterization of solid remainder, Bioresource Technology, 185, pp. 21–27. https://doi.org/10.1016/j.biortech.2015.02.052

Yuan, H., Peng, J., Ren, T., Luo, Q., Luo, Y., Zhang, N., Huang, Y., Guo, X. and Wu, Y., (2021), Novel fluorescent lignin-based hydrogel with cellulose nanofibers and carbon dots for highly efficient adsorption and detection of Cr(VI), Science of the Total Environment, 760, 143395. https://doi.org/10.1016/j.scitotenv.2020.143395

Wang, P., Meziani, M. J., Fu, Y., Bunker, C. E., Hou, X., Yang, L., Msellek, H., Zaharias, M., Darby, J. P., & Sun, Y. (2021), Carbon dots versus nano-carbon/organic hybrids – dramatically different behaviors in fluorescence sensing of metal cations with structural and mechanistic implications. Nanoscale Advances, 3(8), 2316. https://doi.org/10.1039/d1na00002k

Zhang W, Zhong H, Zhao P, Shen A, Li H, Liu X (2022), Carbon quantum dot fluorescent probes for food safety detection: Progress, opportunities and challenges. Food Control 133:108591. https://doi.org/10.1016/j.foodcont.2021.108591